物 理 化 学 学 报

Acta Phys. -Chim. Sin. **2020,** *36* (1), 1908038 (1 of 7)

[Article] doi: 10.3866/PKU.WHXB201908038 www.whxb.pku.edu.cn

Vapor-Liquid-Solid Growth of Bi_2O_2Se Nanoribbons for High-Performance Transistors

Congwei Tan [1,2,†], Mengshi Yu [1,†], Shipu Xu [1], Jinxiong Wu [1], Shulin Chen [3], Yan Zhao [1,2], Cong Liu [1], Yichi Zhang [1], Teng Tu [1], Tianran Li [1], Peng Gao [3], Hailin Peng [1,2,*]

[1] Center for Nanochemistry, Beijing Science and Engineering Centre for Nanocarbons, Beijing National Laboratory for Molecular Sciences, College of Chemistry and Molecular Engineering, Peking University, Beijing 100871, P. R. China.

[2] Academy for Advanced Interdisciplinary Studies, Peking University, Beijing 100871, P. R. China.

[3] Electron Microscopy Laboratory, International Center for Quantum Materials, School of Physics, Peking University, Beijing 100871, P. R. China.

Abstract: Nanostructured bismuth oxyselenide (Bi_2O_2Se) semiconductor, a two-dimensional (2D) materials with high-mobility, air-stability, and tunable bandgap, has recently emerged as a candidate of channel material for future digital (electronic and optoelectronic) applications. In terms of material morphology, some basic issues will be addressed when a two-dimensional layered crystal is shaped into a one-dimensional (1D) geometry due to size effect; these include the space-confined transport in a plane, which leads to dramatic changes in electronic, optical, and thermal properties. These novel 1D nanostructures with unique properties are an optimal choice for fabricating next-generation integrated circuits and functional devices within the nanometer scale such as gate-all-around field-effect transistors, single-electron transistors, chemical sensors, and THz detectors. As one of the high-mobility 2D semiconductor, 1D high-quality Bi_2O_2Se nanoribbons could be promising for applications in high-performance transistors; however, their synthesis has not been completely developed yet. In our study, we report on the facile growth of Bi_2O_2Se nanoribbons on mica substrates *via* a bismuth-catalyzed vapor-liquid-solid (VLS) mechanism. The preparation of Bi_2O_2Se nanoribbons is based on a previous work that emphasized on the oxidation of Bi_2Se_3 in a chemical vapor deposition (CVD) system and the use of bismuth (Bi) particles as the precursor of Bi catalysis. The morphology, composition, and structure of the as-grown Bi_2O_2Se nanoribbons were characterized by scanning electron microscopy (SEM), atomic force microscopy (AFM), Raman spectroscopy, transmission electron microscopy (TEM), as well as other methods. For a Bi mediated VLS growth process, the growth of Bi_2O_2Se nanoribbons can be self-assembled; further, in this process, as-grown epitaxial Bi_2O_2Se nanoribbons are free-standing with out-of-plane morphology on the mica substrate. Additionally, combining the spherical aberration corrected transmission electron microscope (ACTEM) and selected electron diffraction (SAED) methods, we discovered that the as-synthesized Bi_2O_2Se nanoribbons were single crystalline with high quality. We further investigated the controllable growth for domain size by optimizing the growth temperature of the Bi_2O_2Se nanoribbons. As-synthesized single-crystal Bi_2O_2Se nanoribbons have widths in the range of 100 nm to 20 μm and lengths in the sub-millimeter range. By employing a polymer poly(methyl methacrylate) (PMMA) assisted clean transfer method with the assistance of deionized water, the Bi_2O_2Se nanoribbons can be easily transferred onto a SiO_2/Si substrate. Fabricated into the top-gated field-effect device, the Bi_2O_2Se nanoribbon sample (transferred to the SiO_2/Si substrate) exhibited high electronic performances; these included a high electron mobility of ~220 $cm^2 \cdot V^{-1} \cdot s^{-1}$ at room temperature, good switching behavior with on/off ratio of >10^6, and

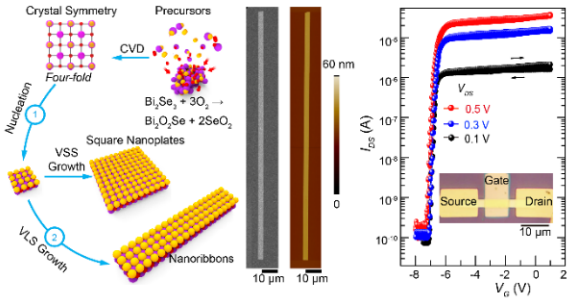

Received: August 29, 2019; Revised: October 11, 2019; Accepted: October 23, 2019; Published online: October 30, 2019.

*Corresponding author. Email: hlpeng@pku.edu.cn.

†These authors contributed equally to this work.

The project was supported by the National Natural Science Foundation of China (21733001, 21525310).

国家自然科学基金(21733001, 21525310)资助项目

high on current density of ~42 μA·μm^{-1} at a channel length of 10 μm. Therefore, Bi_2O_2Se nanoribbons are expected to be a promising materials for building high-performance transistors in the future.

Key Words: Bismuth oxyselenide; Vapor-liquid-solid growth; Nanoribbons; CVD; High mobility

Bi_2O_2Se纳米带的气-液-固生长与高性能晶体管的构筑

谭聪伟[1,2,†]，于梦诗[1,†]，许适溥[1]，吴金雄[1]，陈树林[3]，赵艳[1,2]，刘聪[1]，张亦弛[1]，涂腾[1]，李天然[1]，高鹏[3]，彭海琳[1,2,*]

[1] 北京大学化学与分子工程学院，北京分子科学国家研究中心，北京纳米碳科学与工程中心，纳米化学中心，北京 100871

[2] 北京大学前沿交叉学科研究院，北京 100871

[3] 北京大学物理学院，电子显微镜实验室，国际量子材料中心，北京 100871

摘要：作为一种具有高迁移率、高空气稳定性和带隙可调的二维材料，纳米硒氧化铋(Bi_2O_2Se)半导体有望成为未来电子学集成器件和光电子集成器件沟道材料的候选半导体。高质量的Bi_2O_2Se纳米带有望用于高性能晶体管的构筑；然而，其一维结构的合成方法尚未开发。在我们的研究中，我们在云母衬底上通过Bi催化汽-液-固生长机制合成了一维Bi_2O_2Se纳米带。合成的Bi_2O_2Se单晶纳米带的宽度为100 nm到20 μm，长度可达亚毫米。再者，Bi_2O_2Se纳米带可以很容易地利用洁净转移方法被转移到SiO_2/Si衬底上，并进一步制备成高性能场效应器件。Bi_2O_2Se纳米带场效应器件表现出优异的电学性质：室温电子迁移率高达~220 cm^2·V^{-1}·s^{-1}，开关比高达> 10^6，10 μm沟道长度下电流密度高达~42 μA·μm^{-1}。由此说明，Bi_2O_2Se纳米带有望成为候选材料用于未来高性能晶体管的构筑。

关键词：Bi_2O_2Se；气-液-固生长；纳米带；化学气相沉积；高迁移率

中图分类号：O649

1 Introduction

Fabricating advanced technological-node transistors and manipulating electronic properties of two-dimensional (2D) materials hold significance for their future applications in nanoelectronics, for which converting a two-dimensional to one-dimensional (1D) structure (nanowires, nanotubes, and nanoribbons) is an effective strategy. For future technology nodes, gate-all-around field effect transistors (FETs) fabricated on a 1D semiconductor nanostructure are promising candidates to replace the fin-field effect transistors (FinFETs) Fin Field Effect Transistors and planner short-channel FETs owing to a better electrostatic control of the channel transport and facilitating further reductions in transistor size with low leakage currents *via* fully surrounding gate [1,2]. As the technology node requires to control channel diameter in the sub-3 nm range, except for 2D semiconductor with 1D geometry, most channel materials (Si, Ge and III-V) face process, mobility or quantum capacitance challenges of such ultra-thin body thickness [3,4]. Besides, some basic issues will be addressed as 2D layered crystal shape into a 1D geometry, such as space-confined transport in a plane and leads to dramatic changes in electronic, optical, and thermal properties [1,2,5]. Graphene nanoribbons, as a typical example, varies from pristine 2D graphene nanosheets and exhibits non-zero bandgap useful for room temperature transistor operations with excellent switching speed and high carrier mobility [4,6,7]. Besides, many other ribbon-like 2D materials, such as MoS_2 [8], phosphorene [9,10], WSe_2 [2], and Bi_2Se_3 [11] nanoribbons, also lead to exceptional control over electronic structure, by which the novel quantum phenomena and unique electric properties can be observed. In this regard, fabrication of 2D materials into 1D nanoribbons (varying from the 2D) is capable of arousing scientific and technological interests.

In terms of 2D materials, a currently arising member, bismuth oxyselenide (Bi_2O_2Se), joins the family of layered 2D materials and emerges as a promising candidate for future electronic and optoelectronic applications [12–15]. Bi_2O_2Se has been demonstrated to be of among remarkable characteristics, such as air stability against oxidation and moisture [12], tunable bandgap with the thickness down to a few atomic layers [12,16], high electron mobility (> 20000 cm^2·V^{-1}·s^{-1} at 1.9 K) [12,16–18], being accessible to single crystal films on a wafer-scale [19]. In addition, Bi_2O_2Se exhibits high sensitivity, ultrafast broadband photoresponse (0.3–1.7 μm of wavelength) [13], and ultrabroadband saturable absorption for the mid-infrared (5.0 μm) [20]. Interestingly, a strain may even induce the giant polarizations, resulting in piezoelectricity and ferroelectricity of Bi_2O_2Se [21]. These attractive properties make 2D Bi_2O_2Se became a candidate for creating future infrared photodetector and high-performance electronic devices. Therefore, similar with other 2D materials, it is highly motivated that synthesizing 1D Bi_2O_2Se nanoribbons for realizing potential applications of Bi_2O_2Se among high-performance transistors, but the reliable preparation of Bi_2O_2Se

nanoribbons with chemical method remains challenging.

Here, *via* facial bismuth (Bi)-catalyzed vapor-liquid-solid (VLS) growth mechanism, we present a chemical vapor deposition (CVD) method to synthesize high-quality Bi_2O_2Se nanoribbons. In this mean, Bi is used as catalyst to induce the orientated growth of the Bi_2O_2Se, especially at out-of-plane, resulting in formation of one-dimensional nanoribbons. The bottom-up synthesized Bi_2O_2Se nanoribbons have typical width down to ~100 nm, thickness down to 5 nm and length up to 200 μm. A polymer assisted clean transfer method was developed to transfer the Bi_2O_2Se nanoribbons onto the SiO_2/Si substrate. Fabricated into the FET, the Bi_2O_2Se nanoribbon sample (transferred to the SiO_2/Si substrate) exhibited high electronic performances: high electron mobility of ~220 $cm^2 \cdot V^{-1} \cdot s^{-1}$ and large current on/off ratios of > 10^6.

2 Experimental and computational section

2.1 Synthesis of Bi_2O_2Se nanoribbons

The preparation of Bi_2O_2Se crystal is based on previous work on the oxidation of Bi_2Se_3 in CVD system [16]. Here, we further extend this methodology to prepare Bi_2O_2Se nanoribbons *via* Bi-catalyzed VLS growth. The Bi_2O_2Se nanoribbons were synthesized by the home-made double-zone CVD system (Thermo Inc.), which equipped with a 12-inch-long and 30-mm-diameter quartz tube. Typically, Bi particles (Alfa Aesar, 99.999%) were place in the upstream zone, and Bi_2Se_3 bulks (Alfa Aesar, 99.999%) were place in the second zone. The freshly cleaved mica substrates were place on top of Bi_2Se_3 bulks with a gap of ~3–5 mm. The mixed carrier gas was high-purity Ar/O_2 gas with typical flow rate of 100 sccm/30 ppm (sccm: standard-state cubic centimetre per minute, 1 ppm = 1 × 10^{-6} (volume fraction)), and the pressure of the system was kept at 400 Torr (1 Torr = 133 Pa). The growth range was about 590–620 °C.

2.2 Characterization of Bi_2O_2Se nanoribbons

The morphology of the Bi_2O_2Se nanoribbons was characterized by OM (Olympus DX51 microscope), AFM (Bruker icon), and SEM (Hitachi S4800 field emission). The structure and crystallinity of as-grown Bi_2O_2Se nanoribbons was performed using transmission electron microscopy (TEM, FEI Tecnai F30 and FET Titan Themis G2 operating at 300 kV) with energy-dispersive X-ray (EDX) mapping capabilities. Samples for TEM characterization were transferred onto the carbon film supported gold grids by a polymethyl methacrylate (PMMA)-mediated transfer method with the assistance of deionized water [22]. Raman spectra and mapping was performed at a wavelength of 633 nm on Scanning near-field Raman spectrometer (Witec RSA300+ optical microscope).

2.3 Fabrication of Bi_2O_2Se-nanoribbon-based FET device

To build top-gate FETs, the Bi_2O_2Se nanoribbons were transferred onto 300 nm SiO_2/Si substrates with the location markers using PMMA-mediated transfer method under the assistance of deionized water. The electron beam lithography (EBL, FEI Inc.) was adopted to pattern the electrodes (source, drain, and top-gate electrode) in two steps. Firstly, the source and drain electrodes were patterned with standard EBL process, followed with the metal deposition (Pd/Au, 5 nm/40 nm) by thermal evaporation. Secondly, the top-gated electrodes required a second EBL exposure to exploit the 'window' for the deposition of the high-κ top-gate dielectric HfO_2 (20 nm) by atomic layer deposition (ALD), then 5 nm/40 nm Pd/Au films were deposited as the top-gate electrode. The as-fabricated Bi_2O_2Se-nanoribbon-based top-gate FETs were measured under ambient conditions on a semiconductor analyzer (Keithley, SCS-4200) combined with micromanipulator 6200 probe station at room temperature.

3 Results and discussion

Upon the Vapor-solid-solid (VSS) growth mode, various synthesis process for Bi_2O_2Se generally tends to form 2D structure (square nanoplates) with a characteristic crystal shape [12,16,22–25] (Fig. 1a). In VSS process, determined by the inherent free energy of crystal edges and surface diffusion kinetics, the gas/vapor phase precursors are converted to solid-state products to form the in-plane 2D nuclei *via* surface adsorption on the substrate, resulting in the formation of the native 2D layer structure [8,26]. To prepare 1D morphology, VLS growth is effective mechanism to guide the directed growth of nanostructure, in which 1D nanostructures are synthesized by precipitation from supersaturated catalytic liquid droplets. To this end, we conducted Bi-catalyzed CVD approach to realize VLS growth mode to synthesize the 1D Bi_2O_2Se nanoribbons using Bi_2Se_3 and O_2 as precursors (see Experimental for details). Particularly, there are two advantages for using Bi as a catalyst: (1) Bi acts as a catalyst to realize the VLS growth mechanism for preparation of Bi_2O_2Se nanoribbons [27–30]; and (2) Bi still acts as a reaction precursor to achieve rapid growth of Bi_2O_2Se nanoribbons according to the thermodynamic phase diagram of Bi_2O_2Se [16].

As shown in Fig. 1b, the as-grown crystal shows a ribbon-like

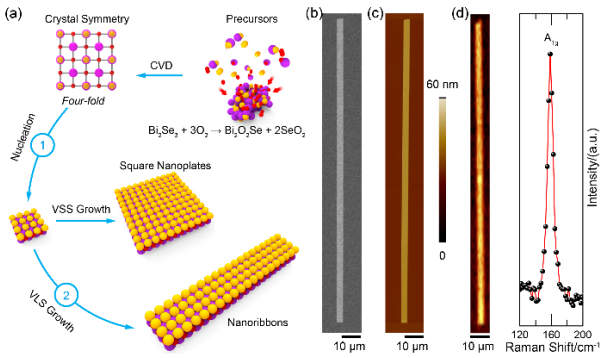

Fig. 1 One-step bottom-up synthesis of Bi_2O_2Se nanoribbons.

(a) Schematic showing growth of Bi_2O_2Se crystals (nanoplates and nanoribbons). (b–d) Scanning electron microscopy (SEM, b), atomic force microscopy (AFM, c), Raman spectra and corresponding mapping (d) images of as-synthesized Bi_2O_2Se nanoribbons.

morphology with the length of sub-millimetre. The atomic force microscopy (AFM) characterization reveals that the surface of the as-grown sample is clean and homogeneous, and its thickness is around 10 nm with a width of 2 μm. Furthermore, Raman spectroscopy indicates that the characteristic A_{1g} peak of Bi_2O_2Se located at ~159 cm^{-1}, which is good consistent with the prior reports [15], confirming that as-synthesized nanostructures are Bi_2O_2Se nanoribbons. In addition, the Raman mapping of A_{1g} peak is very uniform across the whole nanoribbon, demonstrating the high uniformity of as-synthesized Bi_2O_2Se nanoribbons.

To study the phase purity and crystalline nature of as-grown Bi_2O_2Se nanoribbons, we performed characterization of transition electron microscopy (TEM). The as-synthesized Bi_2O_2Se nanoribbons were transferred onto the holey carbon-supported Au grid for TEM characterization *via* a polymethyl methacrylate (PMMA)-mediated method. Low-magnitude TEM image shows that the Bi_2O_2Se nanoribbon has a uniform width along the entire length with typical widths of 500 nm (Fig. 2a). As shown in Fig. 2b, the selected-area electron diffraction (SAED) pattern reveals single set of diffraction peaks with the four-fold symmetry, verifying that it is a single crystal in as-grown Bi_2O_2Se nanoribbon. High-resolution TEM image of the Bi_2O_2Se nanoribbon with a schematic of the atomic positions shows well defined lattice spacing of 0.38 nm, which correspond to the theoretical value of lattice for (100) planes in Bi_2O_2Se [15]. Besides, no obvious defects, such as vacancies, interstitials, and dislocations are observed, suggesting that as-grown Bi_2O_2Se nanoribbons have high crystallinity and purity. As characterized by energy-dispersive X-ray spectrometry (EDS), the obvious signal peaks for Bi, O, and Se were observed (Fig. 2d) without other signal of impurities, the element ratio of Bi, O, Se was about 2 : 2 : 1, which is in accordance with the stoichiometry of Bi_2O_2Se. In addition, corresponding elemental mapping analyses (Fig. 2e) further indicates the uniformity without any impurities, suggesting that the Bi_2O_2Se nanoribbons has good stoichiometry and high purity.

Similarly, some reports have been demonstrated on the catalysis approach for the VLS growth of nanoribbons and nanowire using Bi as catalyst [27–30]. As shown in the scanning electron microscopy (SEM) images (Fig. 3a), as-synthesized Bi_2O_2Se nanoribbons is out-of-plane on the mica substrate, indicating a Bi mediated VLS growth process. Notably, together with TEM analysis, almost no Bi droplets are found at the tip of Bi_2O_2Se nanoribbons, this is owing to the complete evaporation of Bi of the surface during the cooling process [27,28]. Interestingly, although the external perturbation is slight, long and thin out-of-plane Bi_2O_2Se nanoribbons can be easily broke from their root. As indicated in Fig. 3b, c, the as-synthesized thin Bi_2O_2Se nanoribbons quickly broken from their root under the low-voltage SEM irradiation (the voltage is 1 kV). Accordingly, it can be inferred that the nanoribbons on the substrate surface are formed by the fracture of thin out-of-plane Bi_2O_2Se nanoribbons due to the perturbation of cooling process (Fig. 1b and 3d).

The ability to tailor the diameter of Bi_2O_2Se nanoribbons for specific applications is essential for synthetic chemistry. In synthesis of Bi_2O_2Se nanoribbons, varying growth temperature allows considerable control over the diameter of the products. As show in Fig. 3d, the length of as-grown Bi_2O_2Se nanoribbons reached a large value of ~280 μm as temperature varied from

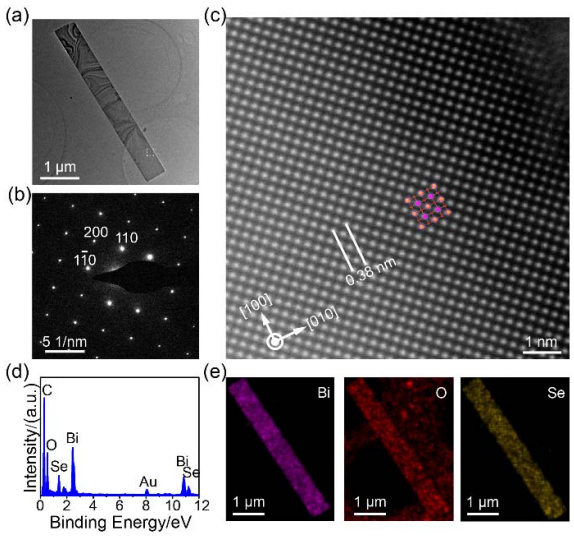

Fig. 2 Structural and crystalline quality characterization of Bi_2O_2Se nanoribbons.

(a) Low-magnitude TEM image of a Bi_2O_2Se nanoribbon that transferred onto the holey carbon-supported Au TEM grid. (b) SAED pattern of as-grown Bi_2O_2Se nanoribbons. (c) Atomically HRTEM images of as-grown Bi_2O_2Se nanoribbons with a schematic of the atomic positions. (d) The EDX spectra of as-synthesized nanoribbons, exhibiting a stoichiometry of Bi_2O_2Se. The Au and C signal comes from the TEM grid. (e) The elemental maps of Bi, Se, and O of as-grown nanoribbons.

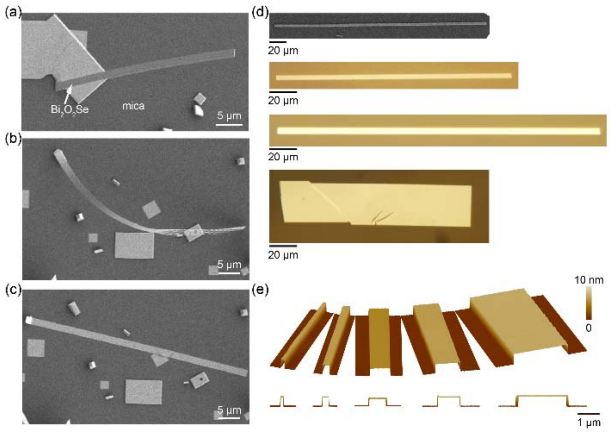

Fig. 3 VLS growth of Bi_2O_2Se nanoribbons on mica substrate.

(a) SEM view images of out-plane Bi_2O_2Se nanoribbons. (b, c) *In situ* SEM images for thin Bi_2O_2Se nanoribbons before and after deformation under the electron beam irradiation. (d) Optical images of as-grown Bi_2O_2Se nanoribbons controlled by the growth temperature, which corresponding to 590 °C (top), 600, 610, 620 °C (bottom), respectively. (e) AFM images of 5 μm long sections of Bi_2O_2Se nanoribbons with widths corresponding to 115 nm, 300 nm, 800 nm, 1.5 μm, 2.4 μm, respectively. Top, 3D view; bottom, the same dataset with the cross view direction through the ribbon length.

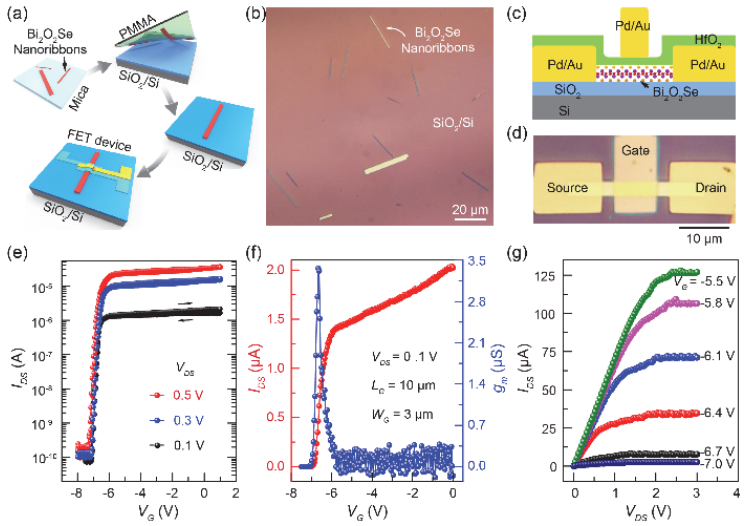

Fig. 4 Fabrication and characterization of FET transistor based on Bi_2O_2Se nanoribbons.

(a) Schematic of fabrication of FET devices *via* the PMMA-assisted transfer method. (b) Optical microscopy image of as-transferred Bi_2O_2Se nanoribbons on SiO_2/Si substrate. (c) Schematic of the top-gate FET devices. (d) Optical image showing an as-fabricated FET with width (W) of 3 μm and gate length (L_G) of 10 μm. (e) Transfer characteristics for drive voltage (V_{DS}) varying from 0.1 to 0.5 V. (f) Transconductance (g_m) and drain current (I_{DS}) as a function of gate voltage (V_G) curves. (g) Output characteristics of FET curves, showing a large on current density (I_{DS}/W) of ~42 μA·μm^{-1}.

590 °C to 610 °C, and it shrank gradually as further increasing the growth temperature. The approximate reason for the above phenomenon can be summarized as follows. There are two other factors that affect the Bi-catalyzed VLS growth: the low vapor pressure of Bi and the rapid reaction of Bi in the presence of oxygen and selenide (the reaction is 4Bi (l) + Se_2 (g) + 2O_2 (g) → 2Bi_2O_2Se (s/l)). When the growth temperature was relatively low, the absorption rate of the Bi-catalyst on the tip of Bi_2O_2Se nanoribbons is relatively high, the catalyzed effect is dominated in VLS process, leading to growth of long and thin nanoribbons. As elevate to high temperature, the evaporation and chemical reaction of Bi is superior to catalyzed effect, the absorption rate of Bi-catalyst diminishes and the catalyzed effect gradually becomes the dominating elemental step for the growth, resulting in wider and shorter of Bi_2O_2Se nanoribbons. Notably, naturally folded without breaking in Bi_2O_2Se nanoribbons can occasionally be formed (Fig. 3d), suggesting that ultrathin nanoribbons are rather flexible. Therefore, upon the aforementioned analysis, as shown in Fig. 3e, we can reliably obtain the thin nanoribbons with different widths and thickness of 5 nm by controlling the growth time under the low temperature (590 °C).

Generally, the direct transfer of Bi_2O_2Se nanoribbons on SiO_2/Si substrates would enable their wide-ranging applications in photonics or electronics because almost all integrated circuits are rooted in the silicon substrate. Hence, as-grown Bi_2O_2Se nanoribbons were firstly transfer onto 300 nm SiO_2/Si substrates to fabricate the FET devices (Fig. 4a). As illustrated in Fig. 4b, as-synthesized Bi_2O_2Se nanoribbons can be easily transfer on SiO_2/Si substrates with various width from Mica substrates, which allow us to evaluate their electronic properties conveniently.

To identify the electronic properties of the nanoribbons, a top-gated device configuration was adopted to evaluate the switching behavior of Bi_2O_2Se nanoribbons with a thickness of 15 nm (Fig. S1, Supporting Information). The structure diagram of Bi_2O_2Se-nanoribbons-based FET devices, and corresponding optical image showing an as-fabricated FET device with a gate length (L_G) of 10 μm and width (W) of 3 μm is shown in Fig. 4c, d, respectively. As shown in Fig. 4e, the measured room-temperature transfer characteristics verify a n-type transistor behavior with a high current on/off ratio (I_{on}/I_{off}) of ~10^6 at low bias (the level of I_{on}/I_{off} is > 10^4 for practical logic transistors) and small subthreshold slope (SS) of ~75 mV·dec^{-1}. Based on the equation $\mu_{FET} = \frac{L}{W C_G} \frac{1}{V_{DS}} \frac{dI_{DS}}{dV_G}$, where L is the channel length (here, L equal to L_G), W is the channel width, C_G is the capacitance between the channel and the top-gate per unit area ($C_G = \varepsilon_0\varepsilon_r/d$, ε_0 is vacuum permittivity, ε_r is the relative permittivity, and d is the thickness of HfO_2 layer), the field-effect mobility of Bi_2O_2Se-nanoribbons-based FET devices could be calculated by fitting the linear region in transfer curve (Fig. 4f). The field-effect mobility was extracted as ~220 cm^2·V^{-1}·s^{-1}, which is the same order as the reported value in a Hall mobility [11,18]. Besides, the output curves plotted in Fig. 4g shows that the high current density (I_{DS}/W) of ~42 μA·μm^{-1} can be achieved. These electronic properties, together with its easy transfer, make Bi_2O_2Se nanoribbons a promising semiconductor candidate for future low-power logic transistors.

4 Conclusions

In conclusion, we have demonstrated the VLS growth of Bi_2O_2Se nanoribbons on Mica substrate *via* Bi-catalyzed CVD. The VLS growth mode is probably conducted by the formation of a Bi liquid solution on the tip of Bi_2O_2Se nanoribbons. The

width and length of Bi_2O_2Se nanoribbons were controlled by tuning the growth condition (growth temperature and time). In particular, the as-grown Bi_2O_2Se nanoribbons can be easily transfer onto arbitrary substrates (such as SiO_2/Si). The high electrical performance (high mobility, high current on/off ratio, and high on current density) of Bi_2O_2Se-nanoribbon-based transistors suggest that Bi_2O_2Se nanoribbons is a promising materials for fundamental investigations and high-performance electronic applications such as Gate-all-around FETs [31,32] and tri-gate FETs [33].

Supporting Information: available free of charge *via* the internet at http://www.whxb.pku.edu.cn.

References

(1) Larrieu, G.; Han, X. L. *Nanoscale* **2013,** *5*, 2437. doi: 10.1039/c3nr33738c

(2) Ryu, M.; Bien, F.; Kim, Y. *AIP Adv.* **2016,** *6*, 015311. doi: 10.1063/1.4940755

(3) Lee, Y.; Luo, G.; Hou, F.; Chen, M.; Yang, C.; Shen, C.; Wu, W.; Shieh, J.; Yeh, W. *IEEE J. Electron Devi.* **2016,** *4*, 286. doi: 10.1109/jeds.2016.2590580

(4) Bangsaruntip, S.; Majumdar, A.; Cohen, G. M.; Engelmann, S. U.; Zhang, Y.; Guillorn, M.; Gignac, L. M.; Mittal, S.; Graham, W. S.; Joseph, E. A.; *et al.* In Gate-all-around silicon nanowire 25-stage CMOS ring oscillators with diameter down to 3 nm. *2010 Symposium on VLSI Technology*, Symposium on VLSI Technology, Honolulu, USA, June 15–17, 2010; Dennison, C., Masaaki, N., Eds.; IEEE, 2010, 21–22. doi: 10.1109/vlsit.2010.5556136

(5) Guo, H.; Lu, N.; Dai, J.; Wu, X.; Zeng, X. C. *J. Phys. Chem. C* **2014,** *118*, 14051. doi: 10.1021/jp505257g

(6) Li, X.; Wang, X.; Zhang, L.; Lee, S.; Dai, H. *Science* **2008,** *319*, 1229. doi: 10.2307/20053480

(7) Schwierz, F. *Nat. Nanotechnol.* **2010,** *5*, 487. doi: 10.1038/nnano.2010.89

(8) Li, S.; Lin, Y. C.; Zhao, W.; Wu, J.; Wang, Z.; Hu, Z.; Shen, Y.; Tang, D. M.; Wang, J.; Zhang, Q.; *et al*. *Nat. Mater.* **2018**, *17*, 535. doi: 10.1038/s41563-018-0055-z

(9) Watts, M. C.; Picco, L.; Russell-Pavier, F. S.; Cullen, P. L.; Miller, T. S.; Bartuś, S. P.; Payton, O. D.; Skipper, N. T.; Tileli, V.; Howard, C. A. *Nature* **2019,** *568*, 216. doi: 10.1038/s41586-019-1074-x

(10) Lee, S.; Yang, F.; Suh, J.; Yang, S.; Lee, Y.; Li, G.; Choe, H.; Suslu, A.; Chen, Y.; Ko, C.; *et al*. *Nat. Commun.* **2015,** *6*, 8573. doi: 10.1038/ncomms9573

(11) Peng, H.; Lai, K.; Kong, D.; Meister, S.; Chen, Y.; Qi, X. L.; Zhang, S. C.; Shen, Z. X.; Cui, Y. *Nat. Mater.* **2009,** *9*, 225. doi: 10.1038/nmat2609

(12) Wu, J.; Yuan, H.; Meng, M.; Chen, C.; Sun, Y.; Chen, Z.; Dang, W.; Tan, C.; Liu, Y.; Yin, J.; *et al*. *Nat. Nanotech.* **2017,** *12*, 530. doi: 10.1038/nnano.2017.43

(13) Yin, J.; Tan, Z.; Hong, H.; Wu, J.; Yuan, H.; Liu, Y.; Chen, C.; Tan, C.; Yao, F.; Li, T.; *et al*. *Nat. Commun.* **2018,** *9*, 3311. doi: 10.1038/s41467-018-05874-2

(14) Quhe, R.; Liu, J.; Wu, J.; Yang, J.; Wang, Y.; Li, Q.; Li, T.; Guo, Y.; Yang, J.; Peng, H.; *et al*. *Nanoscale* **2019,** *11*, 532. doi: 10.1039/c8nr08852g

(15) Yang, J.; Quhe, R.; Li, Q.; Liu, S.; Xu, L.; Pan, Y.; Zhang, H.; Zhang, X.; Li, J.; Yan, J.; *et al. Adv. Electron. Mater.* **2019,** *5*, 1800720. doi: 10.1002/aelm.201800720

(16) Wu, J.; Tan, C.; Tan, Z.; Liu, Y.; Yin, J.; Dang, W.; Wang, M.; Peng, H. *Nano Lett.* **2017,** *17*, 3021. doi: 10.1021/acs.nanolett.7b00335

(17) Tong, T.; Zhang, M.; Chen, Y.; Li, Y.; Chen, L.; Zhang, J.; Song, F.; Wang, X.; Zou, W.; Xu, Y.; *et al. Appl. Phys. Lett.* **2018,** *113*, 072106. doi: 10.1063/1.5042727

(18) Chen, C.; Wang, M.; Wu, J.; Fu, H.; Yang, H.; Tian, Z.; Tu, T.; Peng, H.; Sun, Y.; Xu, X.; *et al. Sci. Adv.* **2018,** *4*, eaat8355. doi: 10.1126/sciadv.aat8355

(19) Tan, C.; Tang, M.; Wu, J.; Liu, Y.; Li, T.; Liang, Y.; Deng, B.; Tan, Z.; Tu, T.; Zhang, Y.; *et al. Nano Lett.* **2019,** *19* (3), 2148. doi: 10.1021/acs.nanolett.9b00381

(20) Tian, X.; Luo, H.; Wei, R.; Zhu, C.; Guo, Q.; Yang, D.; Wang, F.; Li, J.; Qiu, J. *Adv. Mater.* **2018,** *30*, 1801021. doi: 10.1002/adma.201801021

(21) Wu, M.; Zeng, X. C. *Nano Lett.* **2017,** *17*, 6309. doi: 10.1021/acs.nanolett.7b03020

(22) Fu, Q.; Zhu, C.; Zhao, X.; Wang, X.; Chaturvedi, A.; Zhu, C.; Wang, X.; Zeng, Q.; Zhou, J.; Liu, F.; *et al. Adv. Mater.* **2019,** *31*, 1804945. doi: 10.1002/adma.201804945

(23) Li, J.; Wang, Z.; Wen, Y.; Chu, J.; Yin, L.; Cheng, R.; Lei, L.; He, P.; Jiang, C.; Feng, L.; *et al. Adv. Funct. Mater.* **2018,** *28*, 1706437. doi: 10.1002/adfm.201706437

(24) Khan, U.; Luo, Y.; Tang, L.; Teng, C.; Liu, J.; Liu, B.; Cheng, H. M. *Adv. Funct. Mater.* **2019,** *29*, 1807979. doi: 10.1002/adfm.201807979

(25) Wu, J.; Qiu, C.; Fu, H.; Chen, S.; Zhang, C.; Dou, Z.; Tan, C.; Tu, T.; Li, T.; Zhang, Y.; *et al. Nano Lett.* **2019,** *19*, 197. doi: 10.1021/acs.nanolett.8b03696

(26) Wang, S.; Rong, Y.; Fan, Y.; Pacios, M.; Bhaskaran, H.; He, K.; Warner, J. H. *Chem. Mater.* **2014,** *26*, 6371. doi: 10.1021/cm5025662

(27) Yella, A.; Mugnaioli, E.; Panthofer, M.; Therese, H. A.; Kolb, U.; Tremel, W. C. *Angew. Chem. Int. Ed.* **2009,** *48*, 6426. doi: 10.1002/anie.200900546

(28) Xiang, Y.; Cao, L.; Arbiol, J.; Brongersma, M. L.; Fontcuberta i Morral, A. *Appl. Phys. Lett.* **2009,** *94*, 163101. doi: 10.1063/1.3116625

(29) Stanley, S. A.; Stuttle, C.; Caruana, A. J.; Cropper, M. D.; Walton, A. S. O. *J. Phys. D: Appl. Phys*. **2012,** *45*, 435304. doi: 10.1088/0022-3727/45/43/435304

(30) Lee, S. K. C.; Yu, Y.; Perez, O.; Puscas, S.; Kosel, T. H.; Kuno, M. *Chem. Mater.* **2010,** *22*, 77. doi: 10.1021/cm902049p

(31) Loubet, N.; Hook, T.; Montanini, P.; Yeung, C.; Kanakasabapathy, S.; Guillom, M.; Yamashita, T.; Zhang, J.; Miao, X.; Wang, J.; *et al. 2017 Sym. VLSI Technol.* **2017,** T230. doi: 10.23919/vlsit.2017.7998183

(32) Cheng, R.; Liu, B.; Guo, P.; Yang, Y.; Zhou, Q.; Gong, X.; Dong, Y.; Tong, Y.; Bourdelle, K.; Daval, N.; *et al.* Asymetrically Strained High Performance Germanium Gate-All-Around Nanowire p-FETs Featuring 3.5 nm Wire Width and Contractible Phase Change Liner Stressor (Ge_2Sb_2Te5). *2013 IEEE International Electron Devices Meeting*, International Electron Devices Meeting (IEDM), Washington, USA, Dec. 9–11, 2013; Ghani, T., eds.; IEEE, 2013. doi: 10.1109/iedm.2013.6724699

(33) Zhang, C.; Li, X. *Sol. State Electron.* **2014,** *93*, 40. doi: 10.1016/j.sse.2013.12.005